Journal of Sound and Vibration 330 (2011) 5345–5362

Contents lists available at ScienceDirect

Journal of Sound and Vibration

journal homepage: www.elsevier.com/locate/jsvi

Three different guises for the dynamics of a rotating beam

F.S. Buezas [a,b,*], R. Sampaio [c], M.B. Rosales [b,d], C.P. Filipich [d,e]

[a] Department of Physics, Universidad Nacional del Sur, Bahía Blanca, Argentina
[b] CONICET, Argentina
[c] Department of Mechanical Engineering, PUC-Rio, Rio de Janeiro, Brazil
[d] Department of Engineering, Universidad Nacional del Sur, Bahía Blanca, Argentina
[e] CIMTA, FRBB, Universidad Tecnológica Nacional, Bahía Blanca, Argentina

ARTICLE INFO

Article history:
Received 25 August 2010
Received in revised form
23 May 2011
Accepted 26 May 2011
Handling Editor: L.N. Virgin
Available online 8 July 2011

ABSTRACT

The dynamics of a flexible beam forced by a prescribed rotation around an axis perpendicular to its plane is addressed. Three approaches are considered, two of them related with simplified theories, within Strength of Materials, and the third one using Finite Elasticity. In the Strength of Materials approaches, the governing equations of motion are derived by superposing the deformations and the rigid motion in the first model, and in the second by stating the stationarity of the Lagrangian (including first- and second-order effects in order to capture the stiffening due to the centrifugal forces) through Hamilton's principle. Two actions are considered: gravity forces (pendulum) and prescribed rotation. Comparison of the two Strength of Materials models with the model derived from Finite Elasticity is carried out. Predictions for the same problems, interpreted in the context of the specific model, are compared and it was found that sometimes they give rather different results, both in the results and in the computational cost. Energy analyses are performed in order to obtain information about the quality of the numerical solutions. The paper ends with an example of a pendulum with a finite pivot including friction and flexibility. When the structural elements are sufficiently slender and the rotational speeds are low, so that the resulting deformations are small, the Strength of Material model that includes the load stiffening and the Finite Elasticity approach, lead to similar results. It can be concluded that the stiffening phenomenon is appropriately considered in the first model. On the contrary, when the Strength of Material hypothesis are not fulfilled, the problem should be addressed via the Finite Elasticity model. Additionally, cases with complexities such as friction at a finite pivot can only be addressed by Finite Elasticity.

1. Introduction

In the last decade the problem of a plane rotation of a beam has been studied by several authors due to the importance of the problem. There is the possibility of addressing the present problem with models of different levels of complexity. Usually the technical theories start from a simple model and terms are added to account for various effects. In this work two approaches are explored for the study of rotating beams, i.e. Strength of Materials (SM) and Finite Elasticity (FE), or Nonlinear Theory of Elasticity (NLTE). The aim is to compare advantages and disadvantages of both models. The use of a model within the

* Corresponding author. Tel.: +54 291 4595101x2814.
E-mail address: fbuezas@gmail.com (F.S. Buezas).

0022-460X/$ - see front matter © 2011 Elsevier Ltd. All rights reserved.
doi:10.1016/j.jsv.2011.05.035

NLTE frame provides a general tool that allows the validation of the approximated models used in the technical theories. On the other hand, in cases in which the Strength of Materials hypothesis are satisfied, the first method is suitable.

Simo and Vu-Quoc [1] showed that the use of linear-beam theory results in a spurious loss of stiffness due to the partial transfer of centrifugal-force action to the bending equation. Hence, one should account for geometric stiffening (also load stiffening) when the imposed rotation is large. To the best of the authors' knowledge, the first study of vibration of rotating beams was published by Schilhansl [2], who analyzed the bending vibration, assuming steady-state revolution and negligible Coriolis force. He derived a formula relating the fundamental bending eigenfrequency to the angular velocity of revolution. Mayo et al. [3] review different formulations that account for the geometric stiffening effect arising from deflections large enough to cause significant changes in the configuration of the system. El-Absy and Shabana [4] study the effect of geometric-stiffness forces on the stability of elastic and rigid-body modes. A simple rotating-beam model is used to demonstrate the effect of axial forces and dynamic coupling between the modes and the rigid-body motion. In this paper, the effect of higher order terms in the inertia forces as a result of including the longitudinal displacement caused by bending deformation is examined using several models. In [5] the equations of motion are derived by taking into account the foreshortening deformation term, which has geometric stiffening effect on the rigid–flexible coupling dynamics of the system. An influence ratio is employed by Al-Qaisia and Al-Bedoor [6] as a criterion to clarify the application range of the conventional linear modeling method, in which the stiffening effect is neglected. The free bending vibration of rotating tapered beams is investigated using the dynamic stiffness method in [7]. A clamped-free rotating flexible robotic arm is studied by Fung et al. [8]. Hamilton's principle is used to derive the equation of motion of the arm together with the associated boundary conditions and then the power series method is used to solve the differential problem. In other paper, El-Absy and Shabana [9] propose a simple model which demonstrates that there are applications in which the reference motion can have strong dependence on the elastic deformation. The model is used to examine the coupling between the rigid-body and elastic modes. All these authors model the rotating beam with a Strength of Materials theory type, i.e. the dimension of the body (1D) is smaller than the dimension of the embedding space (2D or 3D) (Euler–Bernoulli or Timoshenko equation), assuming plane deformation of the cross-section, and taking into account only the transverse strain. The dynamics of a slender body that is subjected to large displacements can be dealt with models from Strength of Materials (SM) (typically Euler–Bernoulli and Timoshenko equations), or directly by the Theory of Finite Elasticity (see Hunter [10], Truesdell [11,12], Fung [13]).

Almost exclusively, the study of rotational dynamics of a beam is studied from the viewpoint of Euler–Bernoulli or Timoshenko equation (SM) for the transverse displacement and deformation. In this work, we first add the longitudinal deformation of a rotating-beam model according to the theory SM of Euler–Bernoulli and, second, we propose a model based on the FE of the rotating beam, which allows to take into account more complex and realistic phenomena such as dry friction and other types of nonlinear effects due to large deformations. Two types of actions applied to the flexible beam are considered herein. First, the beam is subjected to only gravity forces (i.e. the well-known "pendulum", an object that is attached to a pivot point about which it can swing freely) and second, a rotation of a section of the flexible beam is imposed at the extreme point (a flexible beam subjected to a prescribed rotation means that the speed of rotation will be imposed at a section, in this case the end from which it hangs). Note that, since the body is flexible, the rotation imposed at a section may differ from the rotation at another section. Both cases will be considered by the following three approaches: (a) SM with a floating frame, that is, superposition of a rigid-body motion of the floating frame to small deformation about it, (b) SM via Hamilton's principle including the stiffening contributions and (c) Finite Elasticity (in two dimensions, 2D). In the last case, the constitutive equations are stated using the Piola–Kirchhoff stress tensor (see for instance, Truesdell [12], Fung [13]). The differential equations of motion are developed in Section 2. In Section 3, these equations are presented in the weak form and discretized through finite element via the Galerkin method. The boundary conditions are also discussed given that the equations are stated in a Lagrangian reference in the case of Finite Elasticity. The influence of the stiffening effect in the rotating-beam motion, in the three models are compared. Also, an analysis of the energy conservation is included which permits the control of the numerical convergence. The Finite Elasticity model is taken as a reference. The stiffening effect is shown through the temporal variation of the tip displacement, the natural frequencies, and the mode shapes. Also, the influence on the frequencies of a variation in the Poisson coefficient value is studied using the NLTE approach. It should be noted that the Strength of Materials models do not include this effect. In order to validate this approach, three cases are compared with results found in the literature. A section includes the motion of a 2D pendulum and a comparison with results from the paper of Vetyukov et al. [15], the spin-up maneuver reported in Simo and Vu-Quoc and the roll-up maneuver included by the same authors in [17], in both cases applied to slender beams. Finally, an example of a two body system is included: A pendulum (flexible) with a finite pivot (rigid), exhibiting friction. This last example shows the robustness of a model based on two-dimensional NLTE to get information of complex phenomena. Energy analysis is performed in order to obtain information about the nature of dissipation in the well-know stick-slip phenomena. Section 4 presents some conclusions.

2. Statement of the equations of motion

In this section, the equations of plane motion of a rotating beam are stated and discussed. Three approaches are presented and compared. The first two are Strength of Materials (SM) models for a one-dimension continuum in plane motion and the third one belongs to the two-dimensional nonlinear theory of Elasticity (NLTE), that is the beam is a two-dimensional body in

planar motion. Whereas the stiffening effect is included naturally in the NLTE approach, in the SM theory a second-order effect should be considered to take into account for it.

2.1. Linear one-dimensional model (SM)

Two models are stated within the SM theory. One of them is constructed by superimposing a rigid-body motion of the beam with small deformations around the rigid configuration. The other, stating the stationarity of the action (including the second-order effects in order to capture the stiffening effect) through Hamilton's principle. The superposition and Hamilton's principle models will be named as Model SM1 and Model SM2, respectively.

2.1.1. Model SM1

The governing equations of a beam undergoing plane rotation are stated superposing the equations governing the small deformations of the beam to the ones of the rigid motion [5,7,10]. That is, let us suppose that the body motion is given by the displacement vector $\mathbf{u}=\mathbf{u}_r+\mathbf{u}_d$ where $\mathbf{u}_r(t)=(u_r(t),v_r(t))^{\mathrm{T}}$ is the rigid part of the motion and $\mathbf{u}_d(X,t)=(u_d(X,t),v_d(X,t))^{\mathrm{T}}$ is the part related to the beam elastic deformation. Then the governing equations in the floating frame are [10]

$$EA\frac{\partial^2 u_d}{\partial X^2}-\rho A\left(\frac{\partial^2 u_r}{\partial t^2}+\frac{\partial^2 u_d}{\partial t^2}\right)=f_1 \tag{1}$$

$$EI\frac{\partial^4 v_d}{\partial X^4}+\rho A\left(\frac{\partial^2 v_r}{\partial t^2}+\frac{\partial^2 v_d}{\partial t^2}\right)=f_2 \tag{2}$$

where X is the material coordinate fixed in the frame, t is the time, E is the modulus of elasticity, A is the cross-sectional area of the beam, I is the second area moment, ρ is the volumetric density, $\mathbf{u}=(u,v)^{\mathrm{T}}$ is the displacement vector, u and v are the longitudinal and transverse displacement components, and f_1 and f_2 are the normal and transversely applied forces (gravity components). Now $\mathbf{u}_r$ should be obtained from the equations governing the rigid motion to be replaced in Eq. (2) in order to solve the problem. For instance, in the case of a pendulum of length L and gravity g (see Fig. 1), one obtains $\ddot{\theta}+(3/2L)g\sin\theta=0$, this equation gives $\theta(t)$, and then, $u_r=X(\sin\theta-1)$ and $v_r=-X\cos\theta$ can be computed. For example, if $\mathbf{Q}$ is a point whose coordinates in the inertial system are x and y, and whose coordinate in the rotating frame is X (see Fig. 1), then:

$$\mathbf{Q}=X\begin{pmatrix}\sin\theta\\-\cos\theta\end{pmatrix}=X\hat{\imath} \tag{3}$$

and

$$\ddot{\mathbf{Q}}=X(-\dot{\theta}^2\hat{\mathbf{i}}+\ddot{\theta}\hat{\mathbf{j}}) \tag{4}$$

where $\hat{\mathbf{i}}$ and $\hat{\mathbf{j}}$ are the unit vectors that generate the mobile frame. Then

$$\frac{\partial^2 u_r}{\partial t^2}=-X\dot{\theta}^2,\quad \frac{\partial^2 v_r}{\partial t^2}=X\ddot{\theta} \tag{5}$$

2.1.2. Model SM2

This model is derived by stating the action. The kinematic transformation equations (Fig. 1(a)) are

$$x(X,t)=X\sin\theta+u(X,t)\sin\theta+v(X,t)\cos\theta \tag{6}$$

$$y(X,t)=-X\cos\theta-u(X,t)\cos\theta+v(X,t)\sin\theta \tag{7}$$

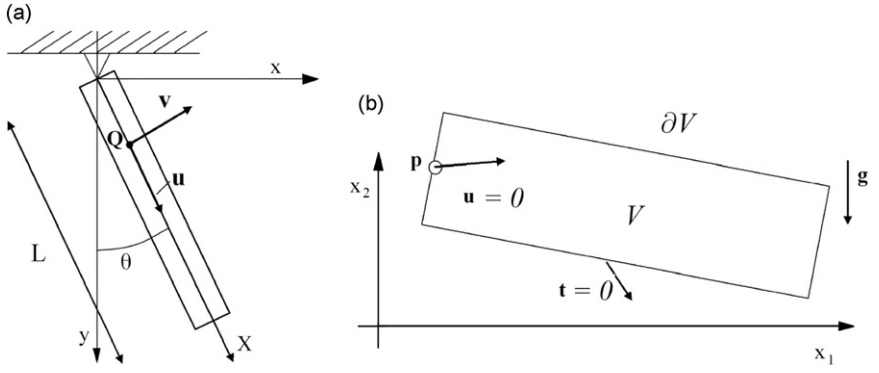

Fig. 1. Geometry of the pendulum. (a) Displacement vectors (SM) and (b) pendulum scheme in the non-deformed configuration (NLTE).

The following four energies contributions are introduced:

$$2W_1 = EA\int_0^L \left(\frac{\partial u}{\partial X}\right)^2 \mathrm{d}X + EI\int_0^L \left(\frac{\partial^2 v}{\partial X^2}\right)^2 \mathrm{d}X \tag{8}$$

$$2W_2 = \int_{(A)}\int_0^L \sigma\left(\frac{\partial v}{\partial X}\right)^2 \mathrm{d}X\,\mathrm{d}A \tag{9}$$

$$2\,K = \rho A\int_0^L (\dot{x}^2+\dot{y}^2)\,\mathrm{d}X, \quad P = -\rho g\int_{(A)}\int_0^L y\,\mathrm{d}X\,\mathrm{d}A \tag{10}$$

where u, v, x, y are functions of (X,t), W_1 is the strain energy due to axial and bending deformations, K is the kinetic energy, P is the gravitational potential energy and W_2 is the internal work done by the axial stress that arise from the centrifugal effect and the change in length due to the bending deformation. The stress due to the centrifugal effect is $\sigma = \rho\omega^2(L^2-X^2)/2$, where ω is the angular velocity. This contribution, well-known within the classical Strength of Materials, is a second-order effect, yet linear. Bleich and Ramsey [18] name this contribution as potential energy of the axial loads. Consequently, the Lagrangian is $\mathcal{L} = K-(W_1+W_2+P)$ and, with this, Hamilton's principle $\delta\int_{t_1}^{t_2}\mathcal{L}\,\mathrm{d}t = 0$ gives the equations of motion

$$k_L\frac{\partial^2 u}{\partial X^2} - (\ddot{u}-\omega^2 u-2\omega\dot{v}) = F(X,t) \tag{11}$$

$$k_v\frac{\partial^4 v}{\partial X^4} + (\ddot{v}-\omega^2 v-2\omega\dot{u}) + \omega^2\left(\frac{X^2-L^2}{2}\frac{\partial^2 v}{\partial X^2} + X\frac{\partial v}{\partial X}\right) = G(X,t) \tag{12}$$

where $\omega = \dot{\theta}$, $k_L = E/\rho$, $k_v = (EI)/(\rho A)$, $F(X,t) = -(\omega^2 X + g\cos\omega t)$, and $G(X,t) = -g\sin(\omega t)$.

2.2. Two-dimensional model with finite deformations (NLTE)

2.2.1. Equations of motion

In this section, the equations of an elastic body in two dimensions for finite displacements and deformations are stated. That is, in these models no hypothesis is made with respect to the size of the deformations. The statement of these equations is made within the frame of the Mechanics of Continuum with the Lagrangian, or material, reference presenting some advantages over the Eulerian, or spatial, reference in the case of Mechanic of Solids problems. In turn, if the problem of the continuum is given by the Eulerian reference, besides the equation of motion (known as Cauchy equation)

$$\mathrm{div}(\boldsymbol{\Sigma}) + \rho\mathbf{b} = \rho\mathbf{a} \tag{13}$$

the mass continuity equation should also be stated

$$\dot{\rho} + \rho\,\mathrm{div}(\mathbf{v}) = 0 \tag{14}$$

where $\boldsymbol{\Sigma}$ is the symmetric Cauchy stress tensor, ρ is the mass density, $\mathbf{b}$ is the body force, and $\mathbf{a}$, $\mathbf{v}$ are the acceleration and velocity fields, respectively, and $\mathrm{div}(\boldsymbol{\Sigma})$ is the divergence of Cauchy stress tensor calculated in spatial coordinates (the same is done for the velocity field). It should be taken into account that both $\mathbf{a}$ and $\mathbf{v}$ are calculated as material derivatives introducing a strong nonlinearity in the differential equations. If the body is subjected to finite displacements in the space, the statement of the boundary equations is a hard problem since the boundary position is one of the unknowns of the motion. Now, if the problem is given in the Lagrangian form, the only vectorial equation of motion to be solved is

$$\nabla\cdot\mathbf{P} + \rho_0\mathbf{b} = \rho_0\mathbf{A} \tag{15}$$

where $\mathbf{P}$ is the first Piola–Kirchhoff stress tensor and $\nabla\cdot\mathbf{P}$ is the divergence of $\mathbf{P}$ calculated in material coordinates [12], ρ_0 is the mass density in the reference (already known), $\mathbf{b}$ is the body force and $\mathbf{A} = \partial\mathbf{V}/\partial t = \partial^2\mathbf{x}/\partial t^2$ where $\mathbf{x} = (x_1,x_2)^{\mathrm{T}}$ is the position vector (spatial coordinate of a material point $\mathbf{X}$) and $\mathbf{A}$ is the acceleration field that is simply the partial derivative of the velocity field $\mathbf{V}$. The boundary conditions are imposed over the reference (always known), which together with the initial conditions and the equation of motion, yield a determined problem. All the nonlinearities are transferred to the non-symmetric $\mathbf{P}$ tensor. The next relationship relates $\mathbf{P}$ and $\boldsymbol{\Sigma}$ (the Cauchy stress tensor—spatial description)

$$\mathbf{P} = \det(\mathbf{F})\boldsymbol{\Sigma}\mathbf{F}^{-\mathbf{T}} \tag{16}$$

where $\mathbf{F}$ is the deformation gradient, $F_{ij} = \partial x_i/\partial X_j$. The second Piola–Kirchoff stress tensor $\mathbf{S}$, which is symmetric, is given by $\mathbf{P} = \mathbf{FS}$. Then, the equation of motion is

$$\nabla\cdot(\mathbf{FS}) + \rho_0\mathbf{b} = \rho_0\mathbf{A} \tag{17}$$

2.2.2. Constitutive equation

The following constitutive law between the second Piola–Kirchhoff stress tensor **S** (symmetric) (**P** = (**FS**)) and the finite strain tensor **E**,

$$\mathbf{E} = \tfrac{1}{2}(\mathbf{F}^{\mathrm{T}}\mathbf{F} - \mathbf{I}) \tag{18}$$

is proposed [13]

$$\mathbf{S}(\mathbf{E}) = \lambda tr(\mathbf{E})\mathbf{I} + 2\mu\mathbf{E} \tag{19}$$

in which λ and μ are Lame's-type constants, $\lambda = vE^*/(1+v)(1-2v), \mu = E^*/2(1+v)$ and E^* and v are constants. Eq. (19) is also known as St. Venant–Kirchhoff material model [11]. Additional alternatives of possible constitutive equations are discussed in Filipich and Rosales [19]. As one can see, **E** is a function of the derivatives of **x**, then by Eq. (19) **S** is also a function of the derivatives of **x**. Similarly, for the tensor **P**, Eq. (15) is

$$\nabla \cdot \mathbf{P}(\mathbf{x}(\mathbf{X},t)) + \rho_0 \mathbf{b} = \rho_0 \frac{\partial^2 \mathbf{x}(\mathbf{X},t)}{\partial t^2} \tag{20}$$

and the goal of this problem is to find the position vector **x** (or displacement vector $\mathbf{u} = \mathbf{x} - \mathbf{X}$) for all **X** and t subjected to the boundary conditions that will be discussed in the next section.

3. Numerical implementation

The following subsections describe the numerical scheme implemented to solve the equations of motion.

3.1. Variational formulation and Galerkin approximation of Model SM1

Let $\boldsymbol{\phi}_j = (\phi_j^1, \phi_j^2)^{\mathrm{T}}$ be a finite element basis (admissible functions), i.e. Adm is a set of trial functions defined as

$$\mathrm{Adm} = \left\{ \begin{array}{l} \phi_j^{1,2} \mid \phi_j^{1,2}(0) = 0, \dfrac{\partial \phi_j^2}{\partial X}\Big| \dfrac{\partial \phi_j^2}{\partial X}(0) = 0 \quad \textit{and}, \\ \displaystyle\int_0^L \left(\frac{\partial \phi_j^1}{\partial X}\right)^2 \mathrm{d}X < \infty, \int_0^L \left(\frac{\partial^2 \phi_j^2}{\partial X^2}\right)^2 \mathrm{d}X < \infty \end{array} \right\} \tag{21}$$

Multiplying Eq. (1) by ϕ_j^1 and integrating by parts, one obtains

$$EA \frac{\partial u_d}{\partial X} \phi_j^1 \Big|_0^L - \int_0^L \left[EA \frac{\partial u_d}{\partial X} \frac{\partial \phi_j^1}{\partial X} + \rho A p_1 \phi_j^1 \right] \mathrm{d}X = 0 \tag{22}$$

with

$$p_1 = \frac{\partial^2 u_r}{\partial t^2} + \frac{\partial^2 u_d}{\partial t^2} - \frac{f_1}{\rho A}$$

In the same way for Eq. (2)

$$EI \left[\frac{\partial^3 v_d}{\partial X^3} \phi_j^2 \Big|_0^L - \frac{\partial^2 v_d}{\partial X^2} \frac{\partial \phi_j^2}{\partial X} \Big|_0^L \right] + \int_0^L \left[EI \frac{\partial^2 v_d}{\partial X^2} \frac{\partial^2 \phi_j^2}{\partial X^2} + \rho A p_2 \phi_j^2 \right] \mathrm{d}X = 0 \tag{23}$$

with

$$p_2 = \frac{\partial^2 v_r}{\partial t^2} + \frac{\partial^2 v_d}{\partial t^2} - \frac{f_2}{\rho A}$$

In the case of a rotating beam, for the pivot point we chose $X=0$, then the essential boundary condition requires that the function satisfy $\phi_j^1 = \phi_j^2 = \partial_X \phi_j^2 = 0$, $\forall j$, and in the free end, $X = L$, the functions $\partial_X u_d = \partial_X^3 v_d = \partial_X^2 v_d = 0$, are then

$$\begin{aligned} -EA \frac{\partial u_d}{\partial X} \phi_j^1 \Big|_0^L &= 0 \\ -EI \frac{\partial^3 v_d}{\partial X^3} \phi_j^2 \Big|_0^L &= 0 \\ EI \frac{\partial^2 v_d}{\partial X^2} \frac{\partial \phi_j^2}{\partial X} \Big|_0^L &= 0 \end{aligned} \tag{24}$$

Then, the goal of this problem is to find $\mathbf{u_d} = (u_d, v_d)^{\mathrm{T}}$ such that

$$\begin{cases} u_d, v_d \in \mathrm{Adm} \\ \forall \phi_j^1 \in \mathrm{Adm} \Rightarrow \int_0^L \left[EA \dfrac{\partial u_d}{\partial X} \dfrac{\partial \phi_j^1}{\partial X} + \rho A p_1 \phi_j^1 \right] \mathrm{d}X = 0 \\ \forall \phi_j^2 \in \mathrm{Adm} \Rightarrow \int_0^L \left[EI \dfrac{\partial^2 v_d}{\partial X^2} \dfrac{\partial^2 \phi_j^2}{\partial X^2} + \rho A p_2 \phi_j^2 \right] \mathrm{d}X = 0 \end{cases} \tag{25}$$

Now, expanding u and v in terms of ϕ_i

$$u = \sum_{i-1}^{N} \phi_i^1(X) C_{i1}(t), \quad v = \sum_{i-1}^{N} \phi_i^2(X) C_{i2}(t) \tag{26}$$

and replacing in Eqs. (22) and (23) we find the matrix forms

$$\mathbf{M}\ddot{\mathbf{C}}_\mathbf{1} + \mathbf{K_1 C_1} = \mathbf{Q_1} \tag{27}$$

$$\mathbf{M}\ddot{\mathbf{C}}_\mathbf{2} + \mathbf{K_2 C_2} = \mathbf{Q_2} \tag{28}$$

where

$$M_{ij} = \rho A \int \phi_i^\alpha \phi_j^\alpha \, \mathrm{d}X, \quad \alpha = 1,2$$

$$K_{1ij} = EA \int \frac{\partial \phi_i^1}{\partial X} \frac{\partial \phi_j^1}{\partial X} \, \mathrm{d}X, \quad K_{2ij} = EI \int \frac{\partial^2 \phi_i^2}{\partial X^2} \frac{\partial^2 \phi_j^2}{\partial X^2} \, \mathrm{d}X$$

$$Q_{1j} = -EA \frac{\partial u_d}{\partial X} \phi_j^1 \Big|_0^L + \int \left[f_1 - \rho A \frac{\partial^2 u_r}{\partial t^2} \right] \phi_j^1 \, \mathrm{d}X$$

$$Q_{2j} = EI \left[-\frac{\partial^3 v_d}{\partial X^3} \phi_j^2 \Big|_0^L + \frac{\partial^2 v_d}{\partial X^2} \frac{\partial \phi_j^2}{\partial X} \Big|_0^L \right] + \int \left[f_2 - \rho A \frac{\partial^2 v_r}{\partial t^2} \right] \phi_j^2 \, \mathrm{d}X$$

3.2. Galerkin approximation of Model SM2

As before, let $\phi_j = (\phi_j^1, \phi_j^2)^{\mathrm{T}}$ be a finite-element basis of a finite dimension subspace of Adm, the space defined by the essential boundary conditions, and using Eq. (26). Multiplying Eq. (11) by ϕ_j^1 and Eq. (12) by ϕ_j^2 and then integrating by parts, or directly from $\delta \int_{t_1}^{t_2} \mathcal{L} \, \mathrm{d}t = 0$, we obtain the matrix forms

$$\mathbf{M}(\ddot{\mathbf{C}}_\mathbf{1} - \boldsymbol{\omega}^\mathbf{2} C_1) - 2\omega \mathbf{A}\dot{\mathbf{C}}_\mathbf{2} + \mathbf{K_1 C_1} = \mathbf{Q_1} \tag{29}$$

$$\mathbf{M}(\ddot{\mathbf{C}}_\mathbf{2} - \boldsymbol{\omega}^\mathbf{2} \mathbf{C_2}) - 2\omega \mathbf{A}\dot{\mathbf{C}}_1 + (\mathbf{K_2} + \mathbf{K}^*)\mathbf{C_2} = \mathbf{Q_2} \tag{30}$$

when

$$M_{ij} = \int \phi_i^\alpha \phi_j^\alpha \, \mathrm{d}X, \quad \alpha = 1,2$$

$$A_{ij} = \int \phi_i^1 \phi_j^2 \, \mathrm{d}X$$

$$K_{1ij} = k_L \int \frac{\partial \phi_i^1}{\partial X} \frac{\partial \phi_j^1}{\partial X} \, \mathrm{d}X, \quad K_{2ij} = -\omega^2 \int (L^2 - X^2) \frac{\partial \phi_i^2}{\partial X} \frac{\partial \phi_j^2}{\partial X} \, \mathrm{d}X$$

$$K_{ij}^* = k_v \int \frac{\partial^2 \phi_i^2}{\partial X^2} \frac{\partial^2 \phi_j^2}{\partial X^2} \, \mathrm{d}X$$

$$Q_{1j} = k_L \frac{\partial u}{\partial X} \phi_j^1 \Big|_0^L - \int F \phi_j^1 \, \mathrm{d}X$$

$$Q_{2j} = \left[-\left(k_v \frac{\partial^3 v}{\partial X^3} + (L^2 - X^2) \frac{\partial v}{\partial X} \right) \phi_j^2 \Big|_0^L + k_v \frac{\partial^2 v}{\partial X^2} \frac{\partial \phi_j^2}{\partial X} \Big|_0^L \right] + \int \left[G - \rho A \frac{\partial^2 v_r}{\partial t^2} \right] \phi_j^2 \, \mathrm{d}X$$

Once more, in the case of a rotating beam, at the pivot point $X=0$ the function $\phi_j^1=\phi_j^2=\partial_X\phi_j^2=0$, $\forall j$ and at the free end ($X=L$) the functions $\partial_X u=k_v(\partial_X^3 v)+(L^2-X^2)\partial_X v=\partial_X^2 v=0$; then the boundary conditions are

$$\left.\frac{\partial u}{\partial X}\phi_j^1\right|_0^L=0$$

$$-\left.\left(k_v\frac{\partial^3 v}{\partial X^3}+(L^2-X^2)\frac{\partial v}{\partial X}\right)\phi_j^2\right|_0^L=0 \tag{31}$$

$$\left.\frac{\partial^2 v}{\partial X^2}\frac{\partial\phi_j^2}{\partial X}\right|_0^L=0$$

3.3. Variational formulation of the problem NLTE

The variational formulation of the equations of motion is straightforward. Let $\mathbf{W}$ be a test vector field (admissible functions) of variables referred to the body in its non-deformed configuration (Lagrangian description). Once again, multiplying the equations of motion by $\mathbf{W}$ and integrating over V_0 we get:

$$\int(\nabla\cdot\mathbf{P}+\rho_0\mathbf{b}-\rho_0\mathbf{A})\cdot\mathbf{W}\,\mathrm{d}V_0=0 \tag{32}$$

$$\int_{\partial V}(\mathbf{t}_0\cdot\mathbf{W})\,\mathrm{d}A_0+[\rho_0(\mathbf{b}-\mathbf{A})\cdot\mathbf{W}-\mathbf{P}\cdot\nabla\mathbf{W}]\,\mathrm{d}V_0=0 \tag{33}$$

where (33) is obtained after integrating (32) by parts (using Green's formula) and $\mathbf{t_0}$ is the stress vector. Here ∂V is the boundary of the region V_0 occupied by the body. The surface integral is divided into two parts, ∂V^1 and ∂V^2. Suppose that the displacement $\mathbf{u}$, and consequently $\mathbf{x}$, is prescribed in a part of the boundary's surface (∂V^1, where the essential boundary conditions are imposed) and the stress is given at the other part (∂V^2). We will see now how to incorporate the boundary conditions

$$\mathbf{x}=\overline{\mathbf{x}}\quad\text{on }\partial V^1 \tag{34}$$

$$\mathbf{t}_0=\overline{\mathbf{t}}_0\quad\text{on }\partial V^2 \tag{35}$$

into the problem. In the case of non-homogeneous essential boundary conditions, the solution $\mathbf{x}(\mathbf{X})$ must satisfy Eq. (34) on ∂V^1 but the test function $\mathbf{W}$ must satisfy the homogeneous essential boundary condition. Then, in the variational problem (33), the admissible test functions $\mathbf{W}$ are defined as

$$\mathbf{W}(\mathbf{X})\in\mathrm{Ad}m_1=\left\{\mathbf{W}\mid\mathbf{W}=0\text{ on }\partial V^1\text{ and }\int(\nabla\mathbf{W})^2\,\mathrm{d}V_0<\infty\right\} \tag{36}$$

and the solution $\mathbf{x}(\mathbf{X})$

$$\mathbf{x}(\mathbf{X},t)\in\mathrm{Ad}m_2=\left\{\mathbf{x}\mid\mathbf{x}=\overline{\mathbf{x}}\text{ on }\partial V^1\text{ and }\int(\mathbf{P})^2\,\mathrm{d}V_0<\infty\right\} \tag{37}$$

and the natural boundary conditions are automatically imposed (33). Then the surface integral in Eq. (33) reduces to

$$\int_{\partial V}(\mathbf{t}_0\cdot\mathbf{W})\,\mathrm{d}A_0=\int_{\partial V^2}\overline{\mathbf{t}}_0\cdot\mathbf{W}\,\mathrm{d}A_0 \tag{38}$$

where $\overline{\mathbf{t}}_0$ is the value of the tension $\mathbf{t_0}$ in the boundary.

In the case of a pendulum (beam rotating under gravity) the stresses are null on the external body surface with exception of the pivot point p (see Fig. 1(b)). On the other hand, the problem with prescribed motion (beam with prescribed rotation with constant velocity), the stresses are null on the external body surface with exception of the clamped boundary. At these points, essential conditions are imposed. In the Lagrangian description the stress is given by $\mathbf{t_0}=\mathbf{P}\cdot\mathbf{N}$, where $\mathbf{t_0}$ is the stress vector of Piola–Kirchhoff and $\mathbf{N}$ is the normal vector of the surface in the reference configuration (Fig. 1(b)).

Finally, the variational problem consists in finding the vector $\mathbf{x}(\mathbf{X},\mathbf{t})$, implicit in $\mathbf{P}$, such that

$$\begin{cases}\forall\mathbf{W}\in\mathrm{Ad}m_1,\text{ find }\mathbf{x}\in\mathrm{Ad}m_2,\text{ that satisfies}\\ \int_{\partial V^2}(\overline{\mathbf{t}}_0\cdot\mathbf{W})\,\mathrm{d}A_0=-\int_V[\rho_0(\mathbf{b}-\ddot{\mathbf{x}})\cdot\mathbf{W}-\mathbf{P}(\mathbf{x})\cdot\nabla\mathbf{W}]\,\mathrm{d}V_0\end{cases} \tag{39}$$

and the initial conditions

$$\mathbf{x}(\mathbf{X},t_0)=\mathbf{x}_0(\mathbf{X}),\quad\dot{\mathbf{x}}(\mathbf{X},t_0)=\mathbf{V}_0(\mathbf{X}) \tag{40}$$

3.3.1. Galerkin method and discretization in finite elements

Let $\{\boldsymbol{\phi}_\mathbf{j}\} \in \mathrm{Ad}m_1$ be a basis of a subspace of a Hilbert space. In this paper ϕ_i are shape vector functions. Let the function $\mathbf{x}(\mathbf{X},t_0)$ be expanded in a series of the vectorial functions $\boldsymbol{\phi}_\mathbf{i}(\mathbf{X})$

$$\mathbf{x}(\mathbf{X},t) \simeq \sum_{i=1}^{N} \boldsymbol{\phi}_i(\mathbf{X})\ c_i(t). \tag{41}$$

Here $c_i(t)$ are functions only of time. The admissible vector functions are

$$\boldsymbol{\phi}_i(\mathbf{X}) = [\phi_{x_1 i}(\mathbf{X}), \phi_{x_2 i}(\mathbf{X})]^{\mathrm{T}}$$

Replacing Eq. (41) by (15) and integrating on the whole domain:

$$\int \left[\nabla \cdot \mathbf{P}(\mathbf{x}) + \rho_0 \mathbf{b} - \rho_0 \left(\sum_{i=1}^{N} \phi_i(\mathbf{X})\ \ddot{c}_i(t)\right)\right] \cdot \boldsymbol{\phi}_j(\mathbf{X})\ \ \mathrm{d}V_0 = 0 \tag{42}$$

for j from 1 to n. $\mathbf{P}(\mathbf{x})$ means that the Piola–Kirchhoff stress tensor is calculated from $\mathbf{x}(\mathbf{X},t)$ through constitutive relations (19).

At last, integrating by parts using Green's formula we get

$$\int_{\partial V_j^2} (\mathbf{t}_0(\mathbf{x}) \cdot \boldsymbol{\phi}_j)\ \mathrm{d}A_0 + \int_{V_j} \left[\rho_0 \left(\mathbf{b} - \sum_{\mathbf{i}=\mathbf{1}}^{\mathbf{N}} \cdot \boldsymbol{\phi}_i\ \ddot{c}_i\right) \cdot \boldsymbol{\phi}_j(\mathbf{X}) - P(x) \cdot \nabla \boldsymbol{\phi}_\mathbf{j}\right] \mathrm{d}V_j = 0 \tag{43}$$

where V_j is the volume of the jth element.

If the problem has non-homogeneous essential boundary conditions, the approximations are

$$\mathbf{x}(\mathbf{X},t) \simeq \sum_{i=1}^{N} \boldsymbol{\phi}_i(\mathbf{X})\ c_i(t) + \phi_0(\mathbf{X}) \tag{44}$$

where ϕ_0 is known and $\phi_0 = \overline{\mathbf{x}}$ on ∂V^1, and consequently $\mathbf{x} \in \mathrm{Ad}m_2$.

3.4. Simulation and results

In this subsection the following models will illustrate the three approaches:

1. A flexible beam rotating in a plane under gravity action is studied using Model SM1, i.e. a Strength of Materials approach with superposition of the beam vibrations to the rigid overall motion.
2. A flexible beam subjected to a prescribed rotation is solved using Model SM2. Since the simulations are done for high-speed rotations, the consideration of the stiffening effect is essential. It was introduced by means of a second-order term into the governing functional (Eq. (9)).
3. A flexible beam subjected to both a prescribed rotation and gravity is addressed with Model NLTE.
4. A two body system composed of a flexible pendulum and a finite pivot which is considered rigid is analyzed with the NLTE approach taking into account the friction at the joint.

When dealing with the linear SM models, a cubic finite element basis was employed. On the other hand, a quadratic finite element basis was employed to discretize the spatial domain in all the NLTE simulations. Temporal integration was performed using the Gear method (second-order implicit Backward Difference Formula).

3.4.1. Example 1. The pendulum

The first example deals with a beam with $L = 5$ m, a square cross-sectional area $A = 0.01\ \mathrm{m}^2$, Young's modulus $E = 4 \times 10^7\ \mathrm{Nm}^{-2}$, Poisson coefficient $\nu = 0.3$ and mass density $\rho = 7850\ \mathrm{kg/m}^3$ (Fig. 1). The material properties were chosen to make apparent the differences among the models through larger deformations. The beam is released from a horizontal position with null velocity and restricted to plane motion under the gravitational field. Fig. 2(a) shows the beam motion through 11 instantaneous configurations during the first second of the motion, corresponding to the Model SM1 and Model NLTE with a 2D discretization. Also, the energy variation is depicted in Fig. 2(b). It is seen that the total energy remains constant, a necessary condition for the numerical solution since we are dealing with a conservative system. The total energy E_t is the sum of the kinetic, elastic strain and potential energies, i.e. $E_t = T + U_e + U_g$ with $T = \frac{1}{2}\int \rho_0 \mathbf{V} \cdot \mathbf{V}\ \mathrm{d}V_0$, and $U_g = g \int \rho_0 x_2\ \mathrm{d}V_0$. It can be proved that for the constitutive law (19), the elastic energy takes the following expression [14]:

$$U_e = \int \left[\frac{\lambda}{2} tr(\mathbf{E})^2 + \mu\ tr(\mathbf{E} \cdot \mathbf{E})\right] \mathrm{d}V_0 \tag{45}$$

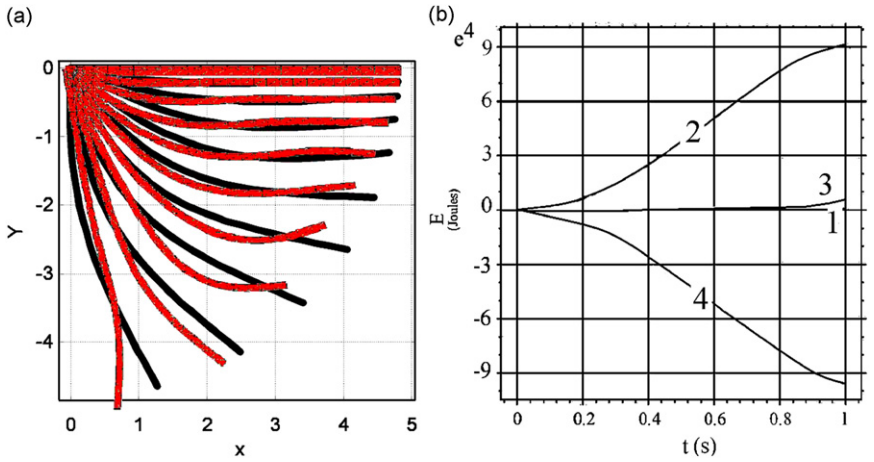

Fig. 2. Example 1. Configuration of the bar at different times. Plots at time intervals $\Delta t = 0.1$ s. (a) Model SM1 (black line) and Model NLTE (2D) (red line). (b) Energy in joules (J) as function of time. (1) Total energy, (2) kinetic energy, (3) strain energy and (4) gravitational potential energy. (For interpretation of the references to color in this figure legend, the reader is referred to the web version of this article.)

Table 1
Duration of numerical experiments with 1D and 2D simulations. Time in seconds.

Simulated time (s)	CPU time (s)		
	1D (SM2)	2D (NLTE)	Ratio 2D/1D
1	10	158	15.8
2	19	304	16

The number of finite elements and the time step were adjusted after an error study. For this purpose the error was defined as follows:

$$\text{error} = \frac{100}{L}\int_V \left[(x_1^m - x_1^{m'})^2 + (x_2^m - x_2^{m'})^2)\right] \mathrm{d}V_0 \tag{46}$$

Superscript m denote the present numerical experiment and superscript m' a reference solution. The reference case was performed with a hundred times more elements and a time step $1/100$ smaller than the m case. The aim was to get results with errors less that 1% at $t=1$ s. The computational time of the reference experiment to simulate the dynamics during the first second was 12,500 s. The duration of the other experiments is depicted in Table 1.

3.4.2. *Example 2. Beam subjected to prescribed rotations*

The numerical simulation of the dynamics of a beam subjected to prescribed rotations is now presented. The beam length is $L=1$ m, the cross-sectional area is 0.01 m^2, the prescribed angular velocity is $\omega = 3000$ rad/s, Young's modulus is $E = 3.4 \times 10^{10}$ Nm^{-2}, the mass density $\rho_0 = 7850$ kg/m^3 and the Poisson coefficient $v = 0.3$. In particular, a large value of ω was assumed in order to obtain large deformations. Thus, the differences among the three approaches could be highlighted. The beam starts its motion from a zero reference (null displacement) and the initial velocity field corresponds to a rigid rotation. That is, the beam begins its motion from a horizontal position ($\mathbf{x}(\mathbf{X},t) = \mathbf{X}$) with a speed given by $V_1 = 0$ and $V_2 = \omega X_1$. The results and comparisons are depicted in Figs. 3 and 4. The temporal variation of the coordinate x_1 at the free end of the beam during the motion is plotted in Fig. 3 in which the values were found with Model SM1, Model SM2, and Model NLTE (2D). The curves are qualitatively similar though the responses found with SM exhibit larger peaks than the NLTE model results. It can be observed that the NLTE leads to a stiffer response. Probably this could be explained due to the choice of a linear Lagrangian constitutive law—$\mathbf{S}(\mathbf{E})$. If the second Piola–Kirchhoff stress tensor $\mathbf{S}$ is transformed into the Cauchy stress tensor Σ, a stiffening behavior with respect to the SM model would arise. This peculiarity is then not due to the rotation event but to the chosen constitutive model. Fig. 4 depicts the variation of the vibration frequency (nondimensionalized with respect to the corresponding frequency at $\omega = 0$) when the rotating velocity is increased. The frequency values were found from a Fast Fourier Transform (FFT) plot. The Model SM1 results are shown in dashed lines, the SM2 are shown in dashed-dot line and the NLTE model in full lines. The results are evidently very close in the cases SM2 and NLTE. The case SM1 is indifferent to the rotation speed as follows directly from Eq. (2). The velocities were assumed small so as to show that the stiffening is not only consistent with the observed physical behavior but that it is

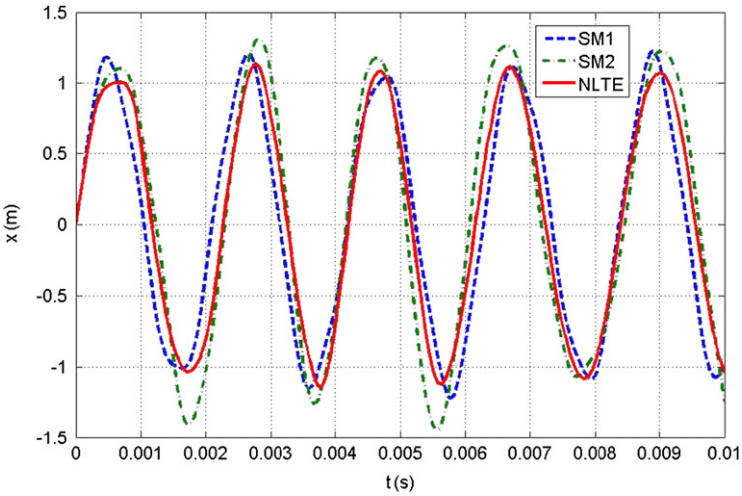

Fig. 3. Example 2. Temporal variation of coordinate x_1 at the beam tip, $X=L$. Comparison of Models SM1, SM2 and NLTE (2D).

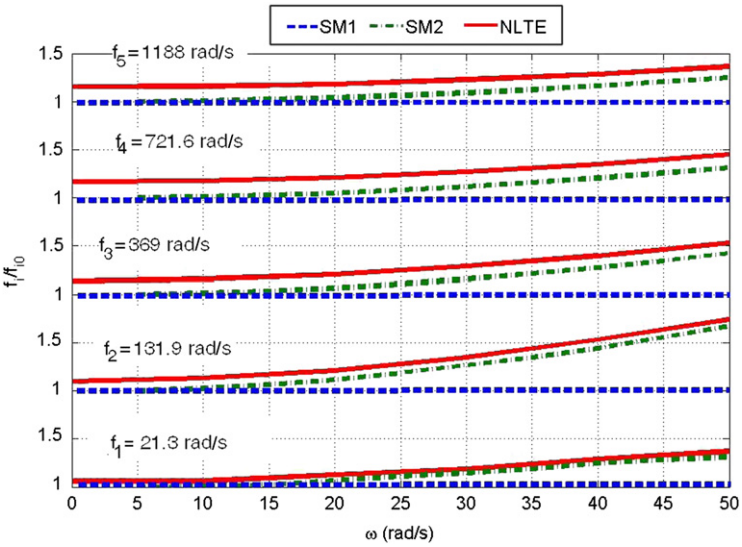

Fig. 4. Example 2. Variation of the first five frequencies with angular velocity ω. Comparison of Models SM1, SM2 and NLTE (2D). The frequencies are normalized to the non-rotating-beam frequency.

Table 2
Example 2. Variation of the first five frequencies (in rad/s) with angular velocity ω with coupled equations via FFT. Comparison of Models SM2 and NLTE (2D).

ω	SM2					NLTE				
	f_1	f_2	f_3	f_4	f_5	f_1	f_2	f_3	f_4	f_5
10	21.56	133..47	372.95	726.82	1203.18	22.65	140.60	388.05	753.50	1226.00
30	24.47	149.85	390.52	747.70	1222.86	25.30	174.75	404.50	770.35	1242.50
50	28.36	176.64	423.29	784.03	1621.2	29.15	180.70	435.00	802.55	1275.00

also consistent with the NLTE model, in the range of small deformations. Some numerical values of this plot are tabulated in Table 2 in order to show the differences between the methods SM2 and NLTE. For example, the difference in the frequencies between SM2 and NLTE when $\omega = 50$ rad/s are 5% for the first mode, 7% for the second, 11% for the third, 14% for the fourth, and 11% for the fifth one. Similar differences are found when $\omega = 0$.

Since mode shapes are defined for linear problems, and the SM1 model does not reproduce the stiffening effect and, on the other hand, the NLTE model is nonlinear, we can only solve the eigenproblem derived from the SM2 model. But, as can be observed from Eqs. (11) and (12) the equations are coupled and yield a nonlinear equation. In order to simplify it and to show representative mode shapes, the coupling terms were neglected and thus, the uncoupled linear eigenproblem was solved for $\omega = 0$, 50, and $\omega = 100$ rad/s. It is observed that the influence of the coupling is very small (c.f. Table 2 with caption of Fig. 5) for these values of angular velocities. Fig. 5 shows the first three modes (bending type).

Among the effects that can be simulated with the NLTE is the influence of the Poisson coefficient. Fig. 6 shows the Poisson effect in the frequencies when the beam is rotating. To highlight this variation, a less slender beam is analyzed. Its cross-sectional area is 0.1 m^2 and the beam is rotating at $\omega = 50$ rad/s. The curves are normalized to the corresponding case of $\nu = 0$, i.e. $f_{i(\nu=0)}$. It is observed that as the Poisson coefficient increases the normalized frequency also increases. Moreover, the behavior is similar for the three frequencies. More slender beams were analyzed and it was found that this effect diminishes as the slenderness of the beam increases.

3.4.3. *Example 3. Comparison of NLTE model with data published for the case of a pendulum*

Results found with the NLTE model of the present work are contrasted with results reported in [15] in which the floating frame of reference approach is used for the analysis of the in-plane oscillations of a suspended rectangular plate. The approach and the computations are different between this reference and the present work although the same formal theory is used. In [15] the rotation of the frame attached to the body is represented with one rotational degree of freedom. Besides, a set of continuous polynomial shape functions form the Ritz approximation of the deformation of the body. In the present study, no floating frame is employed and a quadratic finite-element basis is chosen for the Galerkin discretization. The plate (or beam) dimensions are L=4 m and a cross-sectional area of 1 m^2, mass density $\rho_0 = 7800$ kg/m^3, $\nu = 0.3$, $E = 4 \times 10^7$ N/m^2. The beam was released from the horizontal undeformed position and then, let to oscillate freely in the gravitational field. An interesting comparison was made regarding the rotation angle. Given the approach used in [15] the angle of rotation is used to parametrize the motion of the beam and it is computed solving the dynamical equation. In the present study this angle is not a direct result of the calculations. The angle was measured at each instant as the slope of the straight line that joins the midpoints of both end cross-sections. Fig. 7(a) shows the angle vs. time reported in [15],

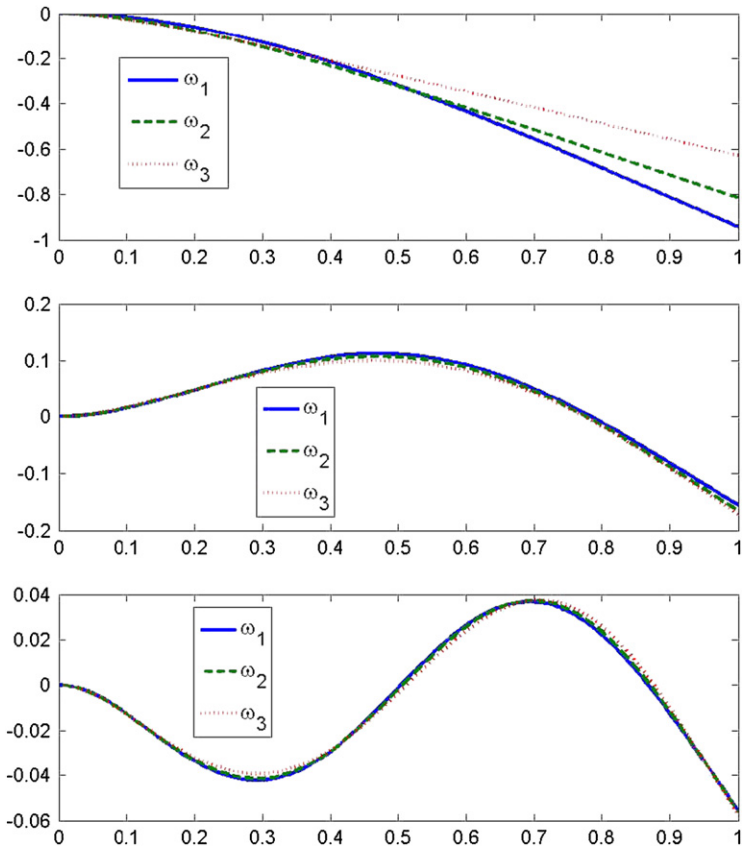

Fig. 5. Example 2. First three mode shapes for the SM2 model. $\omega_1 = 0$ rad/s,$\omega_2 = 50$ rad/s and $\omega_3 = 100$ rad/s. $f_1(\omega_1) = 21.08$, $f_2(\omega_1) = 132.33$, $f_3(\omega_1) = 370.83$, $f_1(\omega_2) = 28.38$, $f_2(\omega_2) = 176.69$, $f_3(\omega_2) = 423.52$, $f_1(\omega_3) = 37.57$, $f_2(\omega_3) = 267.71$, $f_3(\omega_3) = 549.13$ (all frequencies in rad/s), with uncoupled equations.

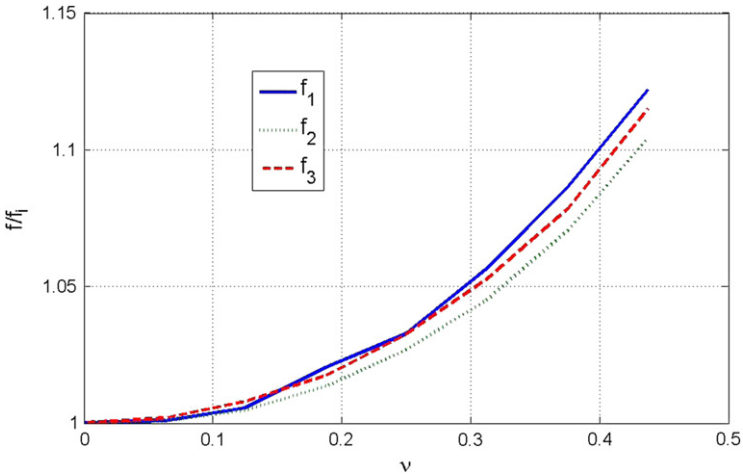

Fig. 6. Poisson effect. Variation of the three first normalized frequencies with ν. $f_1 = 210.8$ rad/s; $f_2 = 1266$ rad/s and $f_3 = 3168$ rad/s.

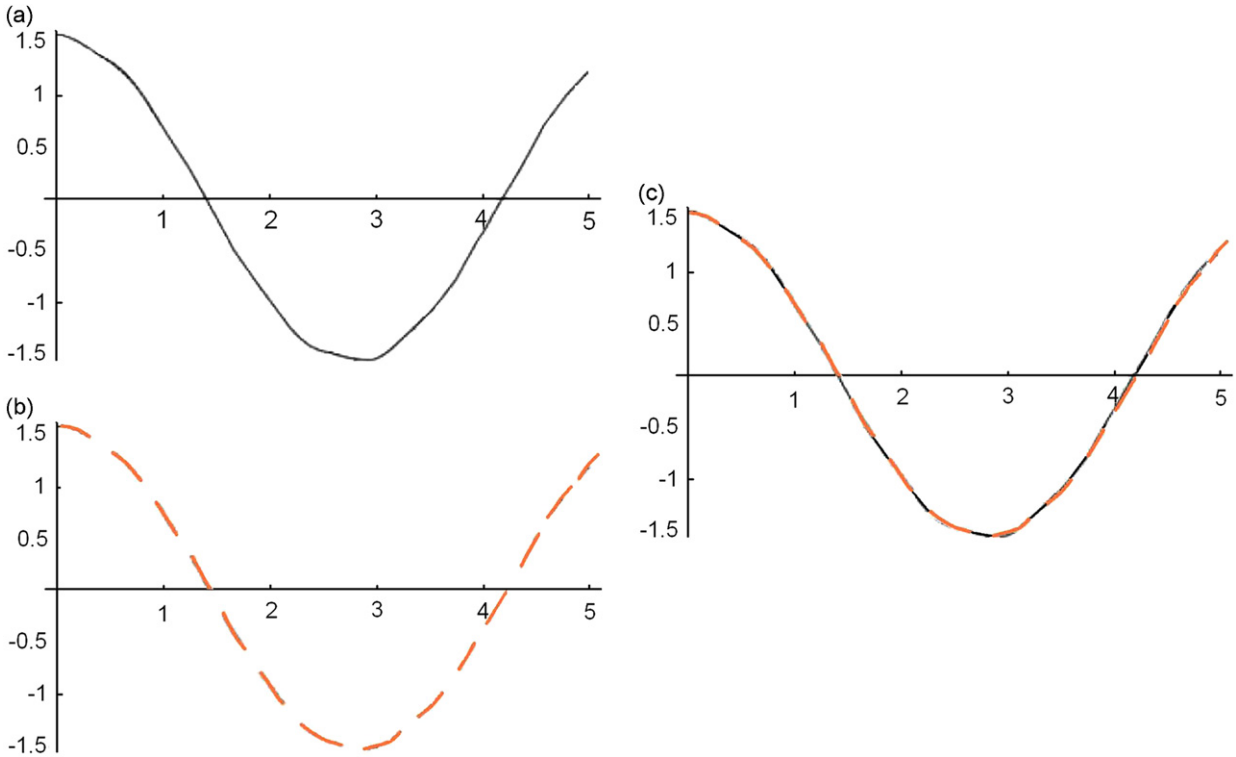

Fig. 7. Example 3. Comparison of Models NLTE (present study) and Ref. [15]. Temporal variation of rotation angle. (a) Vetyukov et al. [15]; (b) present study; (c) superposition of (a) and (b).

Fig. 7(b) plots the resulting angle from the present study and Fig 7(c), the superposition of both results. As is observed, and notwithstanding the diverse methodologies, there is an excellent agreement.

3.4.4. Example 4. Slender beam subjected to a spin-up maneuver

One should account for geometric stiffening (also load stiffening) when the imposed rotation is large. To the best of the authors' knowledge, the first study of vibration of rotating beams was carried out by Simo and Vu-Quoc [1,16,17]. See also the work of Trindade and Sampaio [21] for comment about the Simo–Vu-Quoc model. Additionally, to validate the present beam model based on finite elasticity, and particularly the stiffening effects due to the centrifugal force, a numerical example reported by Simo and Vu-Quoc [16] is herein reproduced, i.e. a flexible beam subjected to a spin-up maneuver by

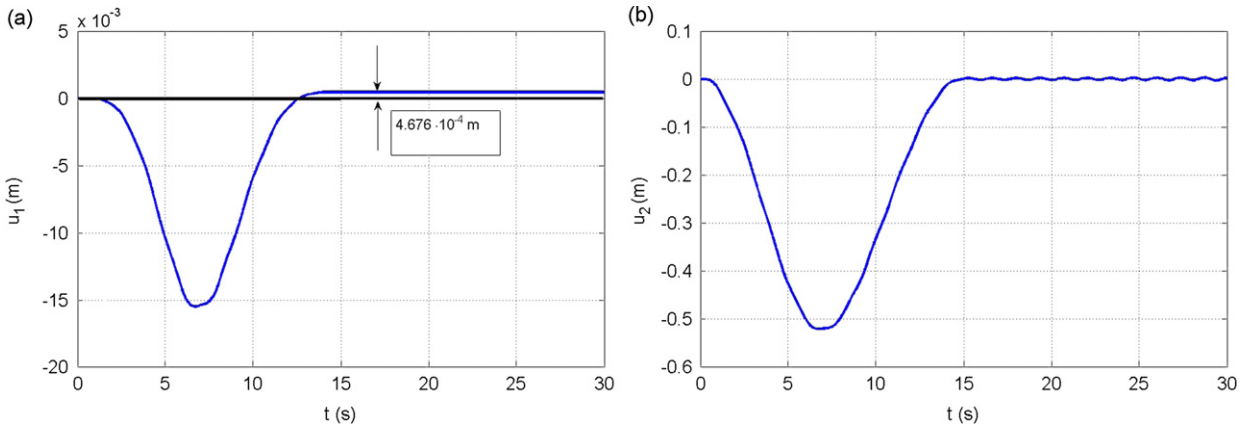

Fig. 8. Example 4. Spin-up maneuver. Time histories of displacement component at the tip of the beam. (a) Axial displacement and (b) transverse tip displacement.

prescribing the angle in one extreme as follows:

$$\phi(t)=\begin{cases}\dfrac{6}{15}\left[\dfrac{t^2}{2}+\left(\dfrac{15}{2\pi}\right)^2\left(\cos\dfrac{2\pi t}{15}-1\right)\right]\ \text{rad}, & 0\le t\le 15\ \text{s}\\ (6t-45)\ \text{rad} & t>15\ \text{s}\end{cases} \tag{47}$$

The data reported in [16] are: $L=10$ m, a cross-sectional area of 0.0775 m^2, mass density $\rho_0=15.4919$ kg/m^3, $\nu=0.3$ (because the beam is very slender, this parameter does not affect the result), and $E=3.6148\times10^8$ N/m^2. The time history of the displacement at the tip of the beam is shown in Fig. 8. Since the NLTE approach of the present study yields the results referred to the material reference, they were transformed to the rotating rigid frame to allow the comparison. Fig. 8(a) depicts the variation of the axial displacement with time during the 30 s experiment. Approximately at $t=12$ s an stationary value of 4.676×10^{-4} m arises which results in a 9% lower than the value reported in [16]. Fig. 8(b) shows the transverse tip displacement. Both curves are very close to the ones reported in the reference paper, despite the different approaches. The small differences may be due to the different constitutive laws in each model. Recall that in the present approach, the constitutive law was stated in terms of the second Piola–Kirchhoff tensor in the Lagrangian reference.

3.4.5. *Example 5. Slender beam subjected to a roll-up maneuver*

The last case analyzed for comparison is the pure bending of a cantilever beam, [17]. A straight rod of unit length of bending stiffness $EI=2$ is subject to a prescribed motion so as to reach a final configuration that is a full closed circle, see Fig. 9. Some additional data necessary in the NLTE model are the modulus of elasticity $E=5\times10^5$ and the height of the beam cross-section in the 2D model, $d=\sqrt[3]{24/E}$. The moment in the tip to make this configuration possible was found to be $M=1.1063(4\pi)$ whereas the value reported in [17] is 4π. Again, this 10% of difference could be explained through the different constitutive laws.

3.4.6. *Pendulum with dry friction in the pivot*

Let us now introduce the dry friction into the model. We model the pendulum hanging from a pivot as a flexible body (it constitutes the cross-section of an axis from which the pendulum hangs, and not as a dimensionless point, that includes friction between pendulum–pivot). As we shall see, the technical one-dimensional models cannot reproduce this type of dynamics because they cannot represent a finite-dimension pivot. This is precisely one of the advantages in the implementation of models that take into account the thickness of rotating systems.

3.4.7. *Modeling of dry friction*

This model was introduced by Amontons in 1699 and was later developed by Coulomb in 1785 [20]. Despite this model gives a rough approximation when dealing with rigid bodies, when it is applied to deformable bodies, it is much more realistic, being able to reproduce phenomena such as the so-called *stick-slip*. The frictional force that a body exerts on another is always less than or equal to a factor μ^* times the normal reaction of the contact surface (called the contact force between two bodies). This frictional force is also collinear and opposite to the sliding velocity of the two bodies:

$$F_T\le\mu^*F_N\rightarrow\begin{cases}\text{if } F_T<\mu^*F_N\Rightarrow & \dot{u}_T=0\\ \text{if } F_T=\mu^*F_N\Rightarrow & \dot{u}_T=-\lambda^*F_T\end{cases} \tag{48}$$

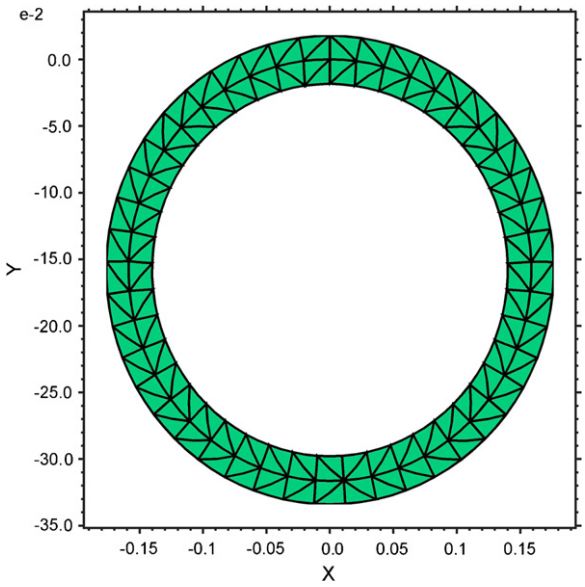

Fig. 9. Example 5. Pure bending of a cantilever beam subject to prescribed motion.

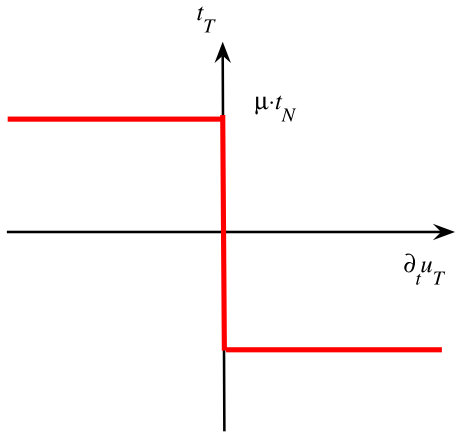

Fig. 10. Friction Law.

where μ^* is the friction coefficient, λ^* is a real number and $\dot{u}_T$ is the tangential component of the velocity. As can be seen, the friction law must be expressed not only in terms of the normal force, but also of the sliding speed. The static friction is contained in the friction law equation (48). See Fig. 10.

$$\mu^* = \begin{cases} \mu_s \text{ if } \dot{u}_T = 0 \\ \mu_d \text{ if } \dot{u}_T \neq 0 \end{cases} \tag{49}$$

In this case, the boundary conditions imposed on the pendulum are the following. (1) In the outer surface, the stress vector is zero. (2) In the pivot of the pendulum, $u_N = 0$ and the tangential component of the stress vector is proportional to the tangential component of the force ($t_T \sim F_T$) (see Fig. 11). Since the friction force depends on the normal force at the pivot (which is unknown) the problem is reformulated so that all boundary conditions are in terms of the stress: assumes that each pivot point (axis) corresponds to a normal stress vector proportional to displacement

$$t_N = -k\, u_N. \tag{50}$$

Then, given a sufficiently large k Eq. (48) may be approximated.

3.4.8. *Regularization of the Coulomb problem*

The friction law formulated in the previous section is non-regular, because there is no univocal functional form that relates t_T with $\dot{u}_T$ for all values of the velocity. For example, when the velocity is zero the friction stress vector is not

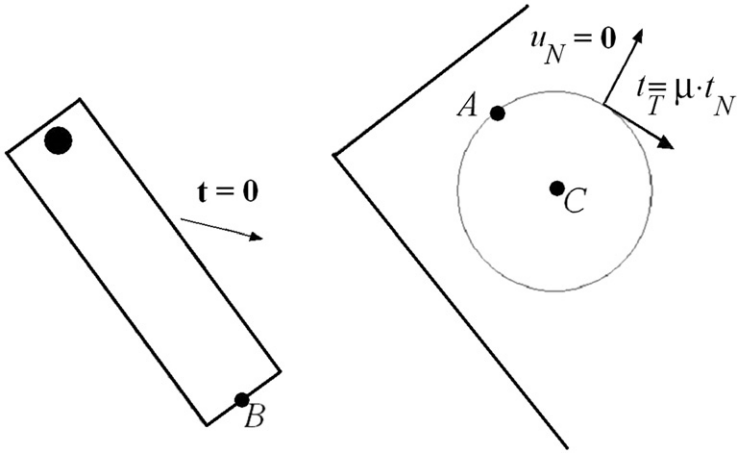

Fig. 11. Boundary conditions for pendulum with finite pivot axis.

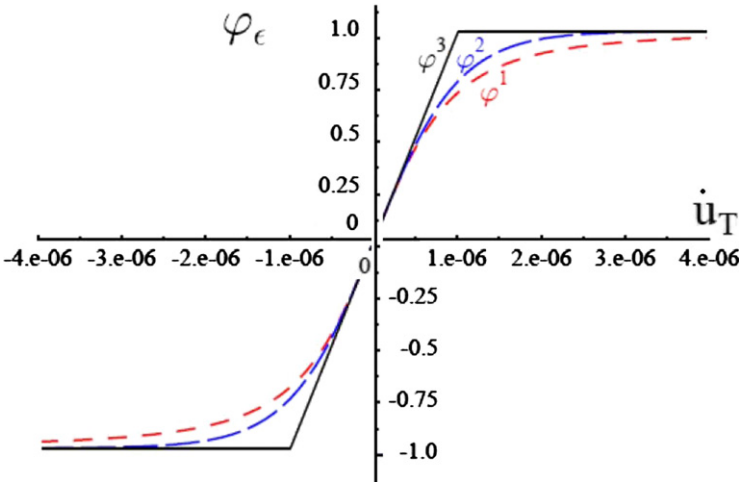

Fig. 12. Regularization performed with different kinds of functions.

defined. For this situation the functional dependence of the friction stress is with respect to other kinematic quantities. However, this law can be regularized,

$$t_T = -\mu^* \phi_\varepsilon(\dot{u}_T)|t_N|. \tag{51}$$

From the numerical point of view this approach will be valid taking ε small enough (Fig. 12). The regularization can be performed with different types of functions. For example, $\phi^1_\varepsilon(\dot{u}_T) = \dot{u}_T/\sqrt{\dot{u}_T^2+\varepsilon^2}$, $\phi^2_\varepsilon(\dot{u}) = \tanh(\dot{u}_T/\varepsilon)$, and defined by parts (the one used in this work)

$$\phi^3_\varepsilon(\dot{u}_T) = \begin{cases} -1 \text{ if } \dot{u}_T < -\varepsilon \\ \dfrac{\dot{u}_T}{2\varepsilon} \text{ if } -\varepsilon < \dot{u}_T < \varepsilon \\ +1 \text{ if } \dot{u}_T > \varepsilon \end{cases} \tag{52}$$

We developed an example to illustrate the influence of the parameters involved, particularly the axis stiffness and friction. A plane pendulum of length $L=1$ m, width $d=0.15$ m, and elastic modulus $E = 6 \times 10^6$ N/m^2 (again, this value is chosen to highlight the phenomenon), $v = 0.3$, rotating around an axis (with finite dimensions) of radius $R = d/4$ centered at $d/2$ from the tip, that is assumed with different flexibilities through values of stiffness k (N/m^3) in Eq. (50). We have also studied the variations in the friction between the pendulum and the axis. The pendulum is released from rest from the horizontal position. We used a 2D model with 132 quadratic elements.

3.4.8.1. Influence of the flexibility of the axis. The time response of the pendulum motion was found for different values of the stiffness of the axis (Eq. (50)): $k=\alpha k_0$ (where $k_0=2\times10^{11}$ N/m and $\alpha=0.1$, 1, 10, 100, 1000). That is, the flexibility of the axis varies, for increasing α, from flexible to more rigid. The influence of this parameter on the motion is shown in Fig. 13(a) (variations in time of x_1 and x_2 coordinates corresponding to point C) (see Fig. 11). It can be seen that if the axis is very flexible (k_1) the point C undergoes significant oscillations. As k increases, becoming more rigid (k_5), this point tends to remain at rest. The effect of flexibility is also visible in Fig. 13(b) that represents the trajectories of point B (at the free end of the pendulum, see Fig. 11) for about half-period for the similar rigid model. It can be seen that for a more flexible axis, the point B has a lower trajectory, as expected.

3.4.8.2. Example 6. Influence of joint friction. The friction between the pendulum and the axis is taken into account with a model of dry friction (Coulomb model). The time response of the pendulum motion was found for different values of μ^*. We consider two coefficients, one static $\mu_s^*=0.7a$ and the other, dynamic $\mu_d^*=0.5a$, where a is a parameter ($a=0.1$, 0.25, 0.5, 0.75, 1). Fig. 14(a)) shows, the temporal variation of the x_1 component of velocity Vx_1 for two values of parameter a (the smallest and the largest, respectively), in all cases with $k=k_5$, and Fig. 14(b) the relation (friction stress)/(normal stress) at point A vs. time (an instantaneous value of friction modulus μ^*). One can see that this ratio alternates between static and dynamic friction, depending on conditions at each instant.

Since the duration of a rigid pendulum period of the same size is about 1 s, every second the pendulum changes its angular velocity and it can be seen that instability occurs (*stick-slip*) due to an alternation between static and dynamic friction. The stick-slip becomes more evident when the friction module increases. Note that after 6 s the instability increases, coinciding with a decrease in the angular velocity of the pendulum. The instability after 6 s is remarkably noticeable in Fig. 14(b).

3.4.8.3. Analysis of energy. Fig. 15 includes the energy change diagrams for a pendulum without friction ($a=0$) and with friction ($a=1$) for $k=k_5$. Note the conservation of total energy in the first case. Similarly to the case of the rigid pendulum, the kinetic energy T is out of phase with the gravitational potential energy U_g. A small part of energy is exchanged with the

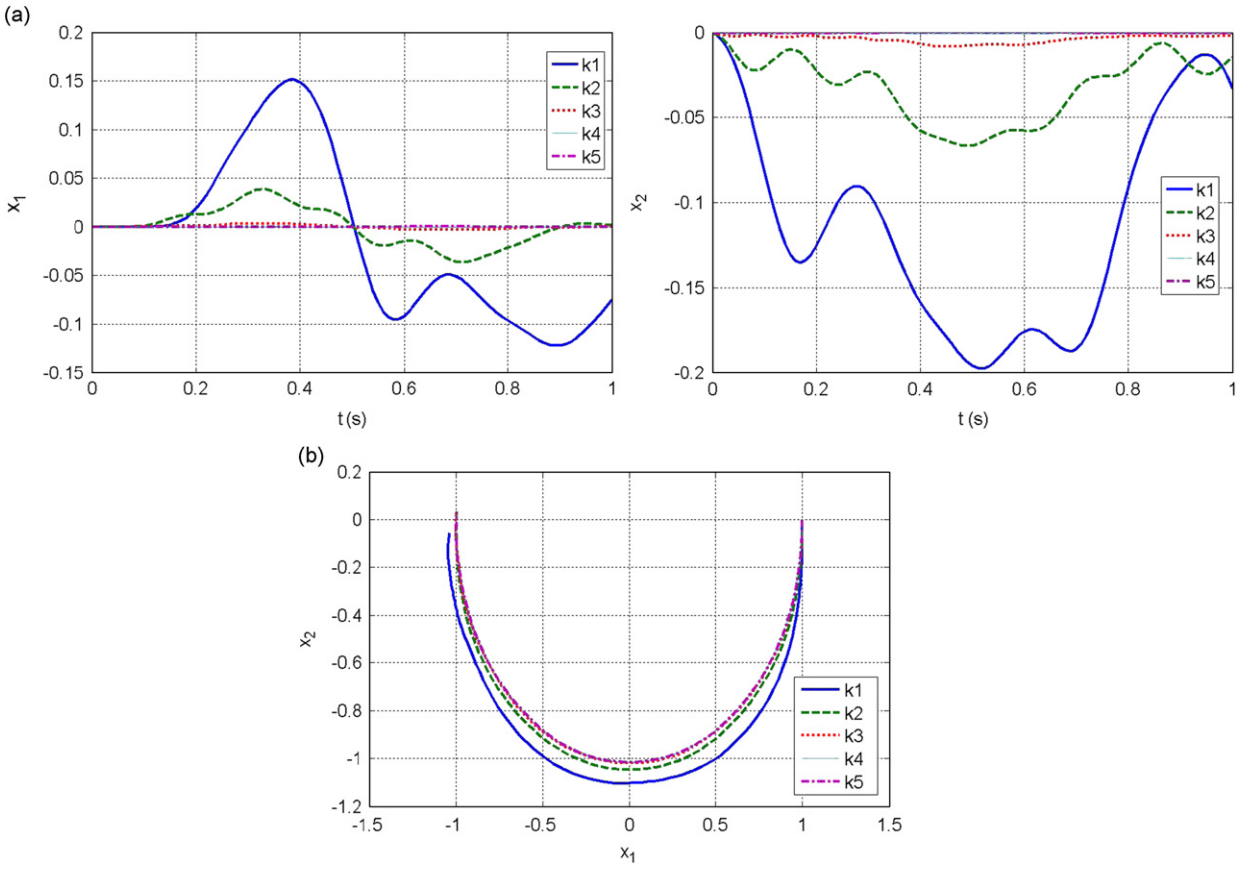

Fig. 13. Example 6. (a) x_1 and x_2 coordinates of point C (axis) over time. (b) Trajectories of point B (the free end of the pendulum).

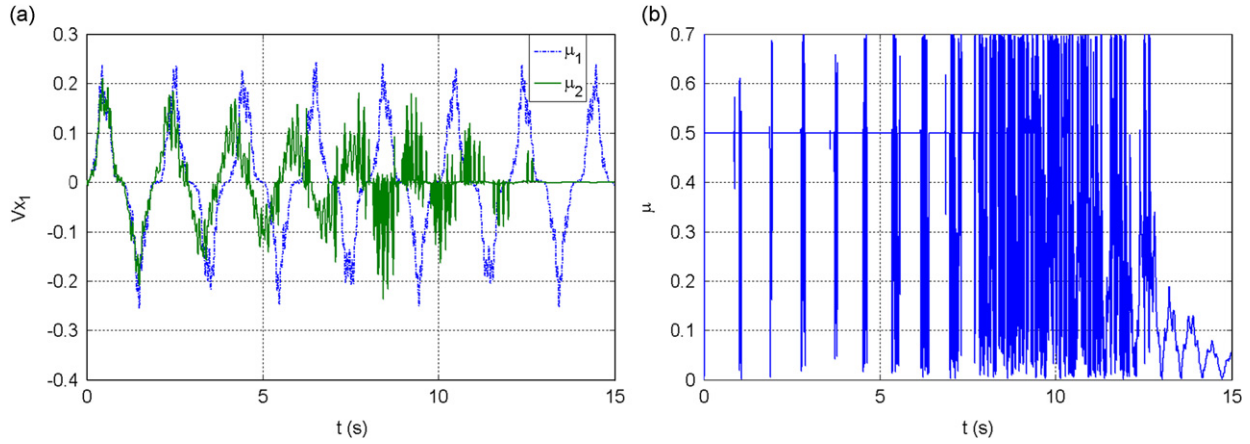

Fig. 14. Example 6. Pendulum with friction. (a) Temporal variation of the x_1 component of velocity $\mathbf{V}_{x_1}$ of point A. (b) Relation (friction stress)/(normal stress) at point A vs. time.

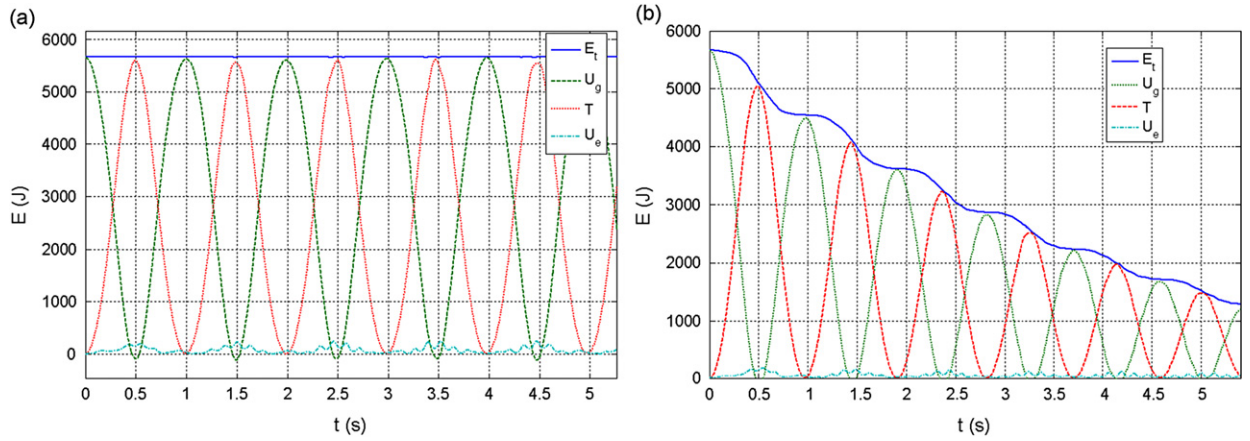

Fig. 15. Example 6. Energy (J) versus time for (a) motion without friction and (b) motion with friction.

elastic energy U_e. This analysis is useful for controlling the quality of the numerical solution because, in this case, the system is conservative. In the other case, the pendulum with friction, one can observe how the energy dissipates.

4. Conclusions

This work has presented a brief review of the literature on the geometric stiffening of rotating flexible beams. Some of the several methodologies proposed in the literature to account for the stiffening effect in the dynamics equations were analyzed. The dynamics of a flexible beam under gravity (pendulum) and with a prescribed rotation were addressed with models of Strength of Material (SM) and the Finite Elasticity (Model NLTE). The SM approach was performed with two models, superposition of motions (Model SM1) and Hamilton's principle (Model SM2), in this both cases, the Poisson ratio v is neglected. The latter included the stiffening effect. In the case of the superposition model, the equations are partially coupled. That is, only the deformation equations are coupled with the rigid motion but the rigid motion equations are uncoupled with the deformations. The nonlinearity is only present in the rigid-body motion. On the other hand, when applying Hamilton's principle, one has fully coupled equations. When the beam is subjected only to gravity, model NLTE yielded similar results to the ones obtained with SM theory (Model SM1). However, in the second example, since a very flexible beam with high rotational velocity was studied, the resulting deformations were not small, and consequently the responses were not identical. Obviously, the more flexible the body, the greater the differences between the linear and the nonlinear models.

A flexible beam undergoing prescribed low-speed rotation was also studied. The stiffening effect in Model SM2 makes it possible to determine almost coincident values of frequencies found via finite deformation Model NLTE. As is well known from experiments, the vibration frequencies of a rotating beam increase as the angular velocity ω increases, which is associated with the stiffening effect introduced by the rotation. In the linear one-dimensional theory (Model SM2) the stiffening effect is due to the contribution of the second-order work done by the axial stress caused by the centrifugal force

over the bending deformation. For the general case of the dynamics of the elastic body considering finite deformation theory of elasticity, it is not necessary to introduce additional terms in the equation of motion. That is, the SM2 theory can not only model the effect of stiffening due to centrifugal force, but also yields similar results than NLTE. This indicates that the stiffening law is correct. In the conservative pendulum case, the total energy composed of the gravitational, strain and kinetic parts remains constant in time. This is useful to check that the integration scheme introduces neither numerical damping nor instabilities in the solutions. The justification for using the full NLTE model is that it includes all effects and allows to tackle complex geometries. Obviously the CPU times are larger. Besides it allows to handle large deformations that can occur with very flexible beams and high rotational speeds. Furthermore, other complexities such a finite-dimensional pivot can be tackled by this approach. This case also includes the phenomenon of friction in the pivot responsible for the so-called *stick-slip*. The energy tracking allows, in this latter case, understanding how energy is dissipated in a flexible pendulum.

Acknowledgments

The authors gratefully acknowledge the support of the Brazilian agencies CNPq and FAPERJ, and the Argentinean agencies CONICET and SGCyT.

.

References

[1] J. Simo, L. Vu-Quoc, The role of non-linear theories in transient dynamic analysis of flexible structures, *Journal of Sound and Vibration* 119 (3) (1987) 487–508.
[2] M.J. Schilhansl, Bending frequency of a rotating cantilever beam, *Journal of Applied Mechanics* 25 (1958) 28–30.
[3] J.M. Mayo, D. Garcia-Vallejo, J. Dominguez, Study of the geometric Stiffening effect: comparison of different formulations, *Multibody System Dynamics* 11 (2004) 321–341.
[4] H. El-Absy, A.A. Shabana, Geometric stiffness and stability of rigid body modes, *Journal of Sound and Vibration* 207 (4) (1997) 465–496.
[5] J.Y. Liu, J.Z. Hong, Geometric stiffening effect on rigid-flexible coupling dynamics of an elastic beam, *Journal of Sound and Vibration* 278 (2004) 1147–1162.
[6] A.A. Al-Qaisia, B.O. Al-Bedoor, Evaluation of different methods of the consideration of the effect of rotation on the stiffening, *Journal of Sound and Vibration* 280 (2005) 531–553.
[7] J.R. Banerjee, H. Su, D.R. Jackson, Free vibration of rotating tapered beams using the dynamic stiffness method, *Journal of Sound and Vibration* 298 (2006) 1034–1054.
[8] E.H.K. Fung, D.T.W. Yau, Effects of centrifugal stiffening on the vibration frequencies of a constrained flexible arm, *Journal of Sound and Vibration* 224 (5) (1999) 809–841 jsvi.1999.2212.
[9] H. El-Absy, A.A. Shabana, Coupling between rigid body and deformation modes, *Journal of Sound and Vibration* 198 (5) (1996) 617–637.
[10] S.C. Hunter, *Mechanics of Continuous Media*, Chichester, Ellis Horwood, 1983.
[11] C. Truesdell, R. Toupin, The classical field theory, *Encyclopaedia of Physics*, Vol. III/1, Springer Verlag, Berlin, 1960.
[12] C. Truesdell, W. Noll, The non-linear field theories of mechanics, *Encyclopaedia of Physics*, Vol. III/3, Springer Verlag, Berlin, 1965.
[13] Y.C. Fung, *Foundations of Solid Mechanics*, Prentice-Hall, New Delhi, 1968.
[14] W.M. Lai, D. Rubin, E. Krempl, *Introduction to Continuum Mechanics*, third ed.,Oxford, New York, Butterworth Heinemann, 1993.
[15] Y. Vetyukov, J. Gerstmayr, H. Irschik, The comparative analysis of the fully nonlinear, the linear elastic and consistently linearized equation of motion of the 2D elastic pendulum, *Computers and Structures* 82 (2004) 863–870.
[16] J.C. Simo, L. Vu-Quoc, On the dynamics of flexible beams under large overall motions—the plane case: part II, *Journal of Applied Mechanics* 53 (1986) 855–863.
[17] J.C. Simo, L. Vu-Quoc, A three-dimensional finite-strain rod model. Part II: Computational aspects, *Computer Methods in Applied Mechanics and Engineering* 58 (1986) 79–116.
[18] F. Bleich, L.B. Ramsey, *Buckling Strength of Metal Structures*, McGraw-Hill, 1952.
[19] C.P. Filipich, M.B. Rosales, A further study on the post-buckling of extensible elastic rods, *International Journal of Nonlinear Mechanics* 35 (2000) 997–1022.
[20] R.E.O. Agamenon, The contribution of Coulomb to applied mechanics, in: *International Symposium on History of Machines and Mechanisms*, Springer, Netherlands 2004, pp. 217–226.
[21] M.A. Trindade, R. Sampaio, Dynamics of beams undergoing large rotations accounting for arbitrary axial deformation, *Journal of Guidance, Control, and Dynamics* 25 (2002) 626–633.